ERROR ANALYSIS OF HYBRID PHOTOVOLTAIC POWER FORECASTING MODELS: A CASE STUDY OF MEDITERRANEAN CLIMATE

Maria Grazia De Giorgi [1], Paolo Maria Congedo, Maria Malvoni, Domenico Laforgia

Dipartimento di Ingegneria dell'Innovazione, Università del Salento, via per Arnesano I-73100, Italy

ABSTRACT

The advancement of photovoltaic (PV) energy into electricity market requires efficient photovoltaic power prediction systems. Furthermore the analysis of PV power forecasting errors is essential for optimal unit commitment and economic dispatch of power systems with significant PV power penetrations. This study is focused on the forecasting of the power output of a photovoltaic system located in Apulia - South East of Italy at different forecasting horizons, using historical output power data and performed by hybrid statistical models based on Least Square Support Vector Machines (LS-SVM) with Wavelet Decomposition (WD). Five forecasting horizons, from 1 h up to 24 h, were considered. A detailed error analysis, by mean error and statistical distributions was carried out to compare the performance with the traditional Artificial Neural Network (ANN) and LS-SVM without the WD. The decomposition of the RMSE into three contributions (bias, standard deviation bias and dispersion) and the estimation of the skewness and kurtosis statistical metrics provide a better understanding of the differences between prediction and measurement values. The hybrid method based on LS-SVM and WD out-performs other methods in the majority of cases. It is also evaluated the impact of the accuracy of the forecasting method on the imbalance penalties. The most accurate forecasts permit to reduce such penalties and thus maximize revenue.

[1] Corresponding author. Tel.: +39 0832297759; fax: +39 0832297777.
E-mail addresses: mariagrazia.degiorgi@unisalento.it

Keywords: Photovoltaic Power Forecast; Least Square Support Vector Machine; Artificial Neural Network; Wavelet Decomposition; Forecasting errors; Imbalance penalties; Solar Irradiance; Weather Variations.

1. Introduction

Productivity forecasting has always been a key issue in power system operation. In particular, with the rise of deregulation and free competition of the electric power industry, loads and productivity forecasting has become more important than ever before. Since renewable energy power plants were used, such as PV systems and wind farm, the productivity forecast for the national energy system becomes difficult due to the high variability of the electricity production of this new system. The present study is a part of the funded research project ‘‘7th Framework Programme Building Energy Advanced Management Systems (BEAMS)’’. The project aims to develop an advanced, integrated management system for many buildings, in particular for the public ones; this system has to be able to control and improve the energy efficiency of infrastructures in term of using public lighting, ventilation, air conditioning, electric vehicles and other types of energy from renewable sources. Furthermore, part of the BEAMS research program concerns the study of the benefits of installation of PV systems and the development of tools to improve/optimize the distribution of loads in the grid composed by the public facility services. The University of Salento is one of the two pilot sites in which this project is being developed [1]. The short term PV power prediction is very important for the planning and management of electric system, but the critical aspects have to be considered. The forecasting accuracy depends also on the weather conditions of installation site and the randomness of solar source is the main limitation of photovoltaic system, which influences the quality of the connected electrical system. The possibility to predict the solar irradiation or PV power (up to 24 h or even more) [2, 3, 4] and the development of real time prediction model [5] help to optimize the integration of PV generator in the electric grids.

The forecasting methods applied in the field of renewable energy can be classified into different categories: the physical model, the conventional statistical model, the spatial correlation model, and the artificial intelligence [6, 7]. Some of these prediction models are more accurate at short-term prediction while others are better in long-term prediction [6].

Electric load time series are usually nonlinear functions of exogenous variables. To incorporate non-linearity, Artificial Neural Networks (ANNs) received great attention in solving problems of electricity price[8], electrical energy consumption [9] or productivity forecasting [10, 11, 12].

In [13, 14, 15] methods based on artificial neural networks were implemented for estimating the energy provided by a PV generator in the next hours. In particular in [15] four different methods were compared: three of them are classical methods and the fourth one is based on an artificial neural network developed by the R&D Group for Solar and Automatic Energy at the University of Jaen.

In the literature different methods based on artificial intelligence techniques have been implemented, including the Artificial Neural Network (ANN) of Multi-Layer Perceptrons (MLP) [16], Radial Basis Function [17] and Recurrent Neural Networks [18] and Adaptive Neuro-Fuzzy Inference Systems (ANFIS) [19].

Studies dealing with the applications of ANNs for PV and wind generation forecasting can be found in [20,21, 22]. In [23] ANNs have been applied for annual energy harvesting calculation of grid-connected PV systems.

Fadare et al. [24, 25] applied ANN model to predict wind speed variation [24] and to forecast solar radiation in Nigeria [25].

Artificial neural network models provide better short-term productivity forecasts with respect to standard linear Autoregressive Integrated Moving Average (ARIMA) models [18] and persistent model [26].

De Giorgi et al. [27] compared ARMA models, which perform a linear mapping between inputs and outputs with Artificial Neural Network (ANNs) and Adaptive Neuro-Fuzzy Inference Systems (ANFIS), which perform a non-linear mapping, underlining that, at long time horizon, ANNs presents higher accuracy in wind power forecasting. This was also confirmed in [28] for PV power predictions.

In [29] Radial Basis Functions and Multilayer Perceptron ANNs were compared to predict solar radiation by estimating the clearness index. To forecast the hourly global horizontal solar radiation, a method, based on the combination of the k-means algorithm and NAR (nonlinear autoregressive) network, was proposed in [30]. In [31] a regression neural network was implemented to predict the solar radiation on tilted surfaces.

In [32] the power forecasting of a PV system was performed by Elman neural network, which was based on solar radiation and weather forecasting data as inputs. However, a major risk in the use of ANN models is the possibility of excessive training data approximation, i.e., over-fitting, which usually increases the out-of-sample forecasting errors.

Recently, new methods for time series forecasting that are based on Learning Machines were developed, using Support Data Machines (SVMs) [33-34]. Several studies underlined that SVMs are more resistant to the over-fitting problem, by achieving high generalization performance in solving forecasting problems of various time series. SVM can model complex problems with datasets given by several variables and a reduced training dataset. In [35] the SVM was used to model the battery nonlinear dynamics. The feasibility of using SVMs to forecast electricity load was discussed in [36]. An advantage in the use of SVM is that it is less computational expensive than traditional ANN models based on back-propagation algorithms [37]. Mohandes et al. [38] compared favorably the performance of SVMs with the multilayer perceptron (MLP) neural networks for the prediction of the wind speed in Madina city, Saudi Arabia.

In [39] the SVM was applied to estimate daily solar radiation using sunshine duration. In [40] an estimation of the monthly solar radiation was obtained by SVM methods that were trained on air temperature data. In [41] the impact of different prediction horizons was evaluated for photovoltaic power forecasting methods, that were based on support vector regression and numerically predicted weather variables.

In the literature various hybrid SVM methods were also developed [42] . An adaptive two-stage hybrid network with self-organized map (SOM) and support vector machine (SVM) was developed for short-term load forecasting in [43].

Beyond the hybridization of the SVM, in the recent literature a variant of the standard SVM has been introduced that is the Least Square Support Data Machine (LS-SVM), which uses a simplified linear model, simpler and computationally easier but with the same advantages of the ANNs and SVMs models [44]. LS-SVM models were already applied for wind power forecasting [45, 46, 47].

Regarding the hybrid methods, prediction forecast models that are based on wavelet decompositions WD, could be used to improve the prediction performance of short-term load forecast, as shown in [48, 49]. Least Square Support Vector Machine (LS-SVM) with Wavelet Transform were used in [50] to predict day-ahead electricity prices.

The PV power time series generally include low and high frequency components. WD decomposes the PV power time series into its components, which could be used separately as input in the prediction model. In [51] a hybrid approach based on WD and ANNs and evolutionary algorithm was successfully proposed for accurate short-term load forecasting of power systems.

Forecasting the produced energy with high accuracy is a key issue in microgrid control, where the photovoltaic (PV) energy sources are dominating the market.

The integration of energy sources into micro-grid operation, as PV generators or wind turbines, needs the consideration of power generation uncertainty. Hence, for optimal operation of PVs and wind turbines, the capacity of solar and wind generation must be considered in the scheduling of the micro-grids. The dependable capacity of PVs and wind turbine is an important factor that is related to the accuracy of photovoltaic and wind power forecast [52].

Finally forecast errors can have substantial economic consequences, if they are large enough that they cause a different commitment than would have been performed with an optimal forecast.

Furthermore, in the liberalized markets, e.g. in Italy [53], if there is a mismatch between the injections of a photovoltaic power plant and the day-ahead market power, the energy injections out of a tolerance band are charged of imbalance penalties [54]. For these reasons, very important is the analysis of the accuracy of the forecasting method by the evaluation of several statistical metrics and of the forecast errors distribution, e.g. the tails of the forecast error distribution have the greatest economic impact and there is more uncertainty in the forecasts.

Despite the importance of a deep analysis of the accuracy of the forecasting methods, several works in the literature performed the evaluation of the different forecasting methods by the estimation of conventional metrics, as the root mean square error (RMSE), mean bias error (MBE), and mean absolute error (MAE). In the present study PV power output forecasting are performed by LS-SVM with Wavelet Decomposition of the input data. Two different input datasets are implemented. The first one is based on the measured power output, the second one uses also the module temperature, the ambient temperature, and the irradiance on plain inclined at the tilt angle. The results in term of accuracy are compared with those of ANN. The performance evaluation is performed by a detailed error analysis [55].

In the literature few works focused on the comparison of ANN and hybrid LS-SVM forecasting models for PV power based on the evaluation of several error metrics.

In the present work a deep study of the statistical error distribution, a decomposition of the standard deviation by amplitude and phase error and the evaluation of the skewness and kurtosis statistical metrics allow to better characterize the performance of LS-SVM and demonstrate that it outperforms ANN methods. The results of the error analysis were also used to evaluated the impact of the accuracy of the forecasting method on the imbalance penalties and costs.

2. PV POWER AND INPUT DATA

The PV park is located in the campus of the University of Salento, in Monteroni di Lecce (LE), Puglia (40° 19'32'''16 N, 18° 5'52'''44 E) that is characterized by a Mediterranean climate. The PV modules were installed on shelters used as car parking, as shown in Fig. 1. The nominal power of PV system is 960kWP by two sub-fields that have the same azimuth (10°) and different tilt of modules (3° and 15°). Technical specifications of the PV module and a detail description of the two subplants are reported in Table 1.

In order to monitor the main parameters of PV system, an integrated data acquisition system is implemented. A set of sensors is used to measure the solar irradiation and the PV module/ambient temperature. Hence, the data are processed and collected by the SCADA System SIMATIC WinCC. The data of PV power are collected every one minute, instead the solar irradiance on the two different tilt modules, the ambient temperature and the module temperature are sampled every 10 minutes. These data are available on the ESAPRO private web site [56].

One of the most important steps in the development of forecasting models is the selection of the input variables that mostly affect the PV power.

The choice of the data, used in the input vector, influences the adequacy of the forecasting methods. A high number of input parameters, called forecasting factors, makes the forecasting system complex, but the use of few input parameters entails an incomplete forecasting model. Therefore it is important to find an adequate choice. In this paper the prediction models implement the historical data series of meteorological parameters as the input vector.

The time series data were recorded from 05/03/2012 to 05/03/2013 every 10 minutes (365 days/8760 hourly records), so the input data were calculated for each hour *i* as follows:

$$F_m(i) = \frac{1}{6}\sum_{t=1*i}^{6} F(t) \qquad i=1,\ldots 8760 \qquad (1)$$

where $F_m(i)$ is the average hourly value of each considered variables, accounting for the previous 60 minutes respect to the hour *i*. The Table 2 summarizes input parameters of the PV system, which were used as forecasting factors for the various prediction models at the five horizons: +1 hour, +3 hours, +6 hours, +12 hours and +24 hours.

As discussed in [55], the use of the input vector given by the historical data of measured PV power, leads to decrease of the performance of the forecasting models. In the present work the impact of the use of the weather parameters in the input vector will be analyzed for both ANN and LS-SVM methods, therefore two different input vectors were chosen based on the following data:

- the average value of the PV power $P_m(i)$ at the i-hour

(IV1) Input Vector 1 $\quad x(i)=[P_m(i)]$ (2)

- the hourly average value of the PV power (kW), module temperature (°C), ambient temperature (°C), irradiance on plain inclined at a tilt angle of 3° and 15° (W/m^2)

(IV2) Input Vector 2 $\quad x(i)=[\, T_m(i); T_a(i); I_3(i); I_{15}(i), P_m(i)]$ (3)

To define the target, the sum of the average hourly powers $P_m(r)$ during the forecast time horizon was considered as:

$$P(i,l) = \sum_{r=i+1}^{i+l} P_m(r) \qquad (4)$$

3. THE PERFORMANCE EVALUATION

To evaluate the forecasting performance, the predicted PV power values were compared with the measured ones. For this aim, several statistical metrics were introduced that explained the average deviations between forecasted and measured data.

3.1 Normalized error

The simplest error measure is the difference between predicted and measured data, to evaluate the degree of similarity between these. Therefore the statistical metrics [55, 57, 58] were considered as follows:

- Normalized error $$E_i(l) = P_N(i,l) - T_N(i,l) \quad (5.a)$$
- Normalized mean bias error (%) $$NMBE(l) = \left(\frac{1}{M} \cdot \sum_{i=1}^{M} E_i(l)\right) * 100 \quad (5.b)$$
- Normalized mean absolute error (%) $$NMAE(l) = \left(\frac{1}{M} \cdot \sum_{i=1}^{M} \left|E_i(l)\right|\right) * 100 \quad (5.c)$$
- Normalized root mean square error (%) $$NRMSE(l) = \sqrt{\frac{1}{M} \cdot \sum_{i=1}^{M} \left(E_i(l)\right)^2} * 100 \quad (5.d)$$

where:

i = generic hour of the predicted data;

l = time horizon;

M = number of predicted data, equal to 1905;

$T_N(i,l) = \frac{\mathrm{T(i,l)}}{Max_{i=1}^{M}(P(i,l))}$, where T(i,l) is the predicted power at hour i for the time horizon l;

$P_N(i,l) = \frac{\mathrm{P(i,l)}}{Max_{i=1}^{M}(P(i,l))}$, where P(i,l) is the measured power used as target at hour i for time horizon, defined as Eq.(4).

3.2 The amplitude and phase error

To understand if the prediction method under or over-estimates the PV power, the standard deviation error SDE is decomposed as the sum of two elements [59]:

$$SDE(l) = \sqrt{\frac{1}{M-1} \cdot \sum_{i=1}^{M} \left(E_i(l) - \hat{E}_i(l) \right)^2} \quad (6.a)$$

$$SDE^2 = SDbias^2 + DISP^2 \quad (6.b)$$

Where

$\hat{E}_i(l)$ is the mean normalized error;

SD_{bias} and DISP are the amplitude and the phase errors.

The amplitude error is due to an overestimation or underestimation of the measured data. The phase error is due to a timing shift of the predicted values with respect to the real data. The SD_{bias} and DISP are defined as:

- Standard deviation bias $$SD_{bias}(l) = \sigma_T(l) - \sigma_P(l) \quad (6.c)$$
- Dispersion $$DISP(l) = \sqrt{2\sigma_T(l)\sigma_P(l)(1 - R_{TP})} \quad (6.d)$$

where:

- $\sigma_T(l)$ = standard deviation of $T_N(i,l)$;
- $\sigma_P(l)$ = standard deviation of $P_N(i,l)$;
- R_{TP} = the cross-correlation coefficient between $T_N(i,l)$ and $P_N(i,l)$.

3.3 The statistical error distribution

To analyze the error distributions, two statistical metrics were introduced: the skewness (SKEW) and the Kurtosis (KURT). The first parameter is a measure of the symmetry of the distribution, or more precisely, the lack of symmetry. If the skewness is negative, the distribution is skewed left. For positive values, the data set is skewed right. If the skewness is near zero, the distribution is symmetric. The second one describes the magnitude of the peak of the distribution and indicates if the data are peaked or flat relative to a normal distribution. Therefore, for high values of the Kurtosis parameter, the distribution has a peak near the mean and decreases rather rapidly with heavy tails. Instead the distribution has a flat trend near the mean rather than a sharp peak in presence of low value of the Kurtosis parameter. These parameters are defined as follows:

$$SKEW = \frac{M}{(M-1)(M-2)} \cdot \sum_{i=1}^{M} \left(\frac{E_i - \hat{E}_i}{SD} \right)^3 \quad (7.a)$$

$$KURT = \left\{ \frac{M(M-1)}{(M-1)(M-2)(M-3)} \cdot \sum_{i=1}^{M} \left(\frac{E_i - \hat{E}_i}{SD} \right)^4 \right\} * \frac{3(M-1)^2}{(M-2)(M-3)} \quad (7.b)$$

4. THE FORECASTING MODELS

This section describes the models that are implemented in this study to forecast the PV power output: the ANN and the LS-SVM. The second one is applied in two configurations, with and without the Wavelet decomposition of the input dataset. The schemes of the different forecasting approaches are shown in Fig. 2.

4.1 Artificial Neural Network

An artificial neural network is similar to the nervous system, through the synapses the electrical impulses move to another neuron. The output signals are the sum of the weighted input signals. A particular function adjusts continuously the weights to obtain the defined accuracy (the training test) [60].

The Elmann network is one of the most popular ANN architecture. It’s a Feed-Forward neural network, in which each layer sends the output to a lower layer. Therefore there is an indirect connection between output and input data. A recurrent connection in the first layer allows the Elman network to detect and generate time-varying patterns. A different activation function allows to define the structure of the Elmann network. The hyperbolic tangent sigmoid transfer function (‘tansig’) is used to hide the neurons in the input and hidden layer of the networks. The ‘purelin’ function activates the neuron in the output layer. During the training of the neural network, the back propagation algorithm is applied, so a gradient descent method establishes the weights. Initially arbitrary weights are chosen and are adjusted in the learning. In this iterative process, a data is input to the network and is propagated forward to determine the output data. The differences between the output data and the real data represent an error. The learning process continues until the network responds with output data, when the Mean Square Error MSE is less than a fixed value [61].

This algorithm updates networks weight and bias values according to gradient descent momentum and an adaptive learning rate, so the Gradient Descent (‘traingdx’) with variable learning rate and momentum weight/bias learning function (‘learngdm’) are utilized. Table 3 summarizes the main Elman ANN settings. A preliminary data analysis was performed to validate available input data. The data were normalized in a range [-1, 1]. The 65% of the collection data are applied as training data sets (8 months), so the residual (35%) are used as test data (4 months).

4.2 Least Squares Support Vector Machine

ANN methods present the disadvantages of the tendency for over-fitting and the enormous computational resources that are required for the training. Lately, alternative methods were investigated as Support Vector Machine [34] that has a well capacity of generalization performance. A different form of SVM algorithm was proposed in [44], called Least Square-Support Vector Machines (LS-SVM), in which the LS-SVM that implements an approach based on Structural Risk Minimization, leads to more generalization and avoids over-fitting. Therefore, LS-SVM is computationally less expensive, since the training requires only the solution of a set of linear equations.

Given a training set of N data points $\{y_k, x_k\}_{k=1}^{N}$, where $x_k \in R^n$ is the k-th input data and $y_k \in R$ is the k-th output data, the following regression model can be constructed by using $\varphi(x_k)$, nonlinear function mapping of the input space to a higher dimensional space:

$$y_k = w\varphi(x_k) + b, \quad k = 1,...,N \tag{8.a}$$

where w is the weight vector and b is the bias term.

The above regression equation is transformed to a quadratic optimization problem with constraint; it means to minimize a cost function J:

$$\min_{w,\xi} J_{LS}(w,\xi) = \tfrac{1}{2} w^T w + \gamma \tfrac{1}{2} \sum_{k=1}^{n} \xi_k^2 \tag{8.b}$$

with ξ_k is an artificial variable, γ is the regularization factor and subject to equality constrains

$$y_k [w^T \varphi(x_k) + b] = 1 - \xi_k, \quad k = 1,..., n \tag{8.c}$$

In order to solve this optimization problem, Lagrange function is defined as:

$$L(w,b,\xi;\alpha) = J_{LS} - \sum_{k=1}^{n} \alpha_k \left\{ y_k [w^T \varphi(x_k) + b] - 1 + \xi_k \right\} \tag{8.d}$$

with $\alpha_k \in R$ is the Lagrangian multipliers,

Solving these equations results into:

$$\min \hat{y} = \sum_{k=1}^{n} \alpha_k K(w, x_k) + b \tag{8.e}$$

Where $\hat{y}$ is the approximated value of y_k and $K(w, x_k)$ is called the kernel function, in the present study the Radial Basis Function kernel RBF is used. More details are reported in [34]. The LS-SVM is tuned by searching the optimal regularization " kernel parameters” as well as the model order, using a 10-fold cross-validation (CV) procedure [44].

4.3 Wavelet Decomposition Technique

Time series of solar irradiance and temperature data include information of daily, seasonal and long-term behaviors; therefore, to improve the forecasting model performance, it would be suitable to use frequency contents of those signals for training, instead of the signal values in itself. To this purpose the forecasting models can be based on wavelet decomposition of the input data.

Wavelet transforms (WT) are time-frequency representations for continuous-time signals. A wavelet is a mathematical function that allows to separate a given function or time signal into different time scale components. It is possible to assign a frequency range to each scale component. The wavelet Φ(t), called mother wavelet of a signal f_k (available at the k-th time interval of n), has a so-called Discrete Wavelet Transform (DWT) defined by:

$$W(m,n) = 2^{-m/2} \sum_{i=1}^{N} f_i \Phi\left((i - N * 2^m)/2^m\right) \tag{9}$$

The scaling and translation parameters are functions of the integer variables *m* and *n* ($a=2^m$, $b=n\cdot 2^m$), where *a* determines the spread of the wavelet and *b* its central position. In the proposed forecast method, a fast DWT algorithm developed by Mallat [48] and based on decomposition and reconstruction low-pass and high-pass filters was used. This algorithm allows to obtain “approximations” and “details” from a given signal. An approximation is a low-frequency representation of the original signal, whereas a detail is the difference between two successive approximations and depicts high-frequency components of the signal.

In the present work the Daubechies type 4 with 8 levels was applied to the time series of input data. The main idea of the algorithm is to use wavelet transform as a pre-processing tool to decompose the original time series into various time scales. This allows the forecasting model, as LS-SVM and

ANN, to learn about the characteristics of the signals at different time scales and to arrive at a model capable of approximating the signal. Fig. 2 shows the implemented algorithm, in which the training and test signals were decomposed using the Wavelet Transform and each decomposed signal was used as single input vector for the Least Quares Support Vector Machine. The final forecast value is given by the sum of the outputs of each forecast on the individual component of the decomposed signal

5. RESULTS AND DISCUSSION

5.1 Analysis of the statistical metrics

This section illustrates the results for the different prediction methods, described previously: the ANN, the LS-SVM and the hybrid LS-SVM with the Wavelet decomposition of the input dataset. For each forecast methodology, the input vector IV1 and IV2 (Eq.2 and Eq.3) are used at several forecast time horizons (1h, 3h, 6h, 12h, and 24h). Table 4 reports the acronyms that are used to identify the various models with the different input vectors.

In Fig. 3 the measured PV power values of a week of the February 2013, which presents high PV power variability are compared with the predicted values of the Model I, II and III based on the inputs IV1 and IV2 at the time horizon equal to 1h. The forecasted power is in quite good agreement with the measured power. The results, which are obtained by all models based on the input IV1, are consistent with the measured power in correspondence of the peaks; even if an over estimation is observed when the power values are close to zero in the model I. It’s also observed that the predicted power time series present a shift on the right. This behavior is less evident when the input IV2 is used, especially at low PV power values.

To deeply analyze and compare the differences between the predicted and the measured power time series, the normalized error E_i is plotted at the time horizons of 6h and 12h, as shown in Fig. 4 and Fig. 5. The chosen week is characterized by power evident fluctuation that allows to underline the impact of the power variations on the errors.

In all cases, the time series of the normalized error follows the trend of the normalized measured PV power, high prediction error values occur when the PV power drastically changes, with an over estimation (positive values of normalized error) when the PV power increases. A negative value of E_i is recorded if the PV power is close to zero. The LS-SVM based on the Wavelet decomposition of the input dataset (Model III) is less sensitive to the variation of the PV power and gives the lowest prediction errors. Training this model with the input vector IV2 increases the prediction accuracy.

To better evaluate the forecasting performance, the statistical metrics that are described in section 3 are determined. Table 5 illustrates the mean error for each model, using the inputs IV1 and IV2. Focusing on the ANN, the NMAE increases in the range 9,40 - 25,05% using the input vector IV1 and 6,50 - 19,60% for the input IV2. In the PV power forecasting by LS-SVM model, the NMAE values are in the range from 7,50 to 23,50% for IV1 and 6,40 – 19,50% for IV2. Furthermore the implementation of the Wavelet decomposition for the input vectors improves the accuracy, in fact the NMAE of the models III.1 and III.2 respectively varies between 6,60 – 15,00% and 6,90 – 19,00%. As expected, the NMAE rises if the time horizon increases and the highest values are for the models based on PV power time series (IV1), in particular for the ANN and LS-SVM without the Wavelet Decomposition. The comparison between NMAE values in the cases of the models I.2 and II.2 shows that the performance of the two models are quite similar. However the best forecasting performances can be obtained if the PV power prediction model is trained on all the available weather parameters (IV2). It is also evident that the use of the Wavelet decomposition of the input vectors reduces the error at long time horizons, particularly for the input vector IV1.

Additional metrics, as the normalized mean bias error and the normalized root mean square error were determined for a more accurate error analysis, as summarized in the Table 5. In Eq.5.d the errors are averaged after they are squared, so the NRMSE assigns a different weight to the errors. The NRMSE is not ever smaller than the NMAE. High difference between NMAE and RMSE indicates that the predicted values are very spread from the measured data. As the NMAE, NRMSE also rises with the prediction length, assuming the lower values in the LS-SVM model with Wavelet decomposition (Model III). Focusing on NMBE, an under-estimation of the PV power is observed for all the time horizons by implementing the model I.1 and II.1; instead the SVM with the Wavelet Decomposition model based on IV1 gives an over-estimation of the PV power.

To evaluate the fluctuations of the error around the mean value, the standard deviation error SDE, as defined in Eq.6.a, was calculated, it rises if the time horizon increases, as shown in Table 6. Models with the input IV2 present lower error variations than the models that were trained on the input IV1. Low values of SDE were obtained for the model III, this confirms the best prediction performance for this model.

Recent power forecasting systems typically take into account systematic errors by estimating the forecast bias (NMBE) and SD_{bias} error and then applying statistical correction schemes prior to analysis. The bias can be subtracted and the SD_{bias} can be adjusted by increasing or decreasing the standard deviation of the prediction, contrary to the phase error.

In the Table 6 the values of SD_{bias} and DISP, as defined in Eq.6.c and Eq.6.d, are also reported. The results underline that all the models tend to under-estimate the PV power (negative values of SD_{bias}) and the amplitude error is higher at long time prediction period. Regarding the dispersion, DISP, the models I and II present the same phase errors for either input vectors, instead its decrease is evident for the predictions of the model III.2. In accordance to Eq.6.b, Fig. 6 reports the value of SDE^2, SD_{bias}^2 and $DISP^2$ that were obtained by training the models with the input IV2. It is evident that the main contribution at the standard deviation error is given by the phase error, especially for short time horizon, with the lowest values for the model III. Increasing the prediction length, the amplitude and phase error also increase, leading to the highest values of SDE^2 at 24h. The SD_{bias} and DISP analysis is in accordance with Fig. 3, their estimation quantify the under or over estimation of the predicted data, and the time shift of predicted PV power time series. The statistical distributions of the power prediction error were reported in Fig. 7 and Fig. 8.

In the forecasting methods that were trained on input IV1 (Fig. 7), the error distributions of the models I and II at short time prediction lengths are quite similar with the most values of the normalized error Ei in the range [-20%, -10 %]. If the error distribution is narrow, the probability that the errors assume low values is higher. When increasing the time horizon, the histograms are shifted on the left, this means that the normalized error has a high probability to assume value in the range [-40%, -20%]. The distributions are more flat at 24h. Instead for the model III the error distributions are quite different, especially for +6h and +12h horizons, the majority of the prediction errors concentrate in the range [-10%, 0].

The statistical distribution of the normalized errors for all the models with input vector IV2 (Fig. 8) is generally narrow with high probability of occurrence in the range of low error values in particular at very short prediction horizons. At 12 and 24 h the distributions don't present high peaks, but cover a wide range of the normalized error.

To characterize the forecast error distribution, the skewness and kurtosis statistics were also calculated and reported in the Table 7 for each prediction horizon and forecasting method. It's noted that the skewness increases for long time horizon with positive value, but at 24 hours it has an inversion of polarity. This means that the error distribution was generally positively skewed at short time horizons and negatively skewed at long horizons. Instead concerning the Kurtosis values, as might be expected, the short time ahead forecasts have much higher kurtosis values than those made at the day-ahead timescale. This would be expected from the reduction in uncertainty that occurs between making a forecast in the day-ahead time frame, versus a single hour ahead. The kurtosis value is positive and decreases with the increase of the horizon, assuming negative value at 24 hours. The distribution is narrow with high peak value at short time horizon, becomes flat at 24 hours. This is in accordance with Fig. 7 and Fig.8.

Comparing the different forecasting methods, it is evident that the forecasts based on LS-SVM present highest kurtosis values from one hour-head up to one-day head.

The probability that the normalized error is in a given error range, focusing on the time horizons of 1h, 6h and 12h, is reported in Table 8, in which the best performances are underlined. For each model, the probability to make an error lower than 1% is less than 45%, and best values, about 20%, are obtained with the model III. Considering the 5%, 10% and 20% confidence intervals, at fixed time horizon the models with the input IV2 present the best results. Therefore, in Fig. 9 the probability error distribution is plotted for all models using input vector IV2. Reducing the confidence interval from 20% to 10%, the probability generally decreases up to 30% at 24h. The probability to make an error smaller than 5% is in a range of 50-60% for short time period and it decreases up to 15% at 24h. The analysis of the probability distributions underlines that the use of the Wavelet decomposition permits an improvement in the power predictions; in particular, at the long time horizons, with highest probability, with respect to other models, in the range of low error values, while at short time horizons best predictions are given by model II.

5.2 Impact of daily weather on prediction errors

The historical data of the solar irradiance are used as input for the forecast models, however the different weather conditions lead to variations of irradiance, hence an analysis has been performed to investigate the effects of the weather fluctuations on the accuracy of the prediction method.

Some significant days have been taken into account in order to evaluate the accuracy forecast methods under different weather conditions. This investigation has been carried out considering the ANN, LS-SVM and LS-SVM model with Wavelet decomposition based on IV2 at two different forecast time horizons (3h and 12h).

Therefore the extraterrestrial solar irradiance G_0 is introduced and defined as follows [62]:

$$G_0 = G_{sc}\left(1 + 0.033\ \cos\frac{360n}{365}\right)\cos\theta_z \quad (10)$$

where

G_{sc} is the solar constant (1367 W/m^2);

n is the day of the year [63];

θ_z is the zenith angle that is the complement of the solar altitude angle α_s ($\theta_z = 90 - \alpha_s$). The extraterrestrial solar irradiance G_0 for the investigated site (Lat. 40°21' Log. 18°11') is shown in Table 9. The zenith angle has been calculated considering the solar altitude angle [64].

Hence to underline the effects of the weather conditions, a comparison between the normalized measured solar irradiance, $I_{15,N}(i)$, on the PV module tilted 15° and the corresponding extraterrestrial solar irradiance $G_{0,N}$ has been performed. The solar irradiance values have been normalized as follows:

$$I_{15,N}(i) = \frac{\mathrm{I}_{15}(\mathrm{i})}{Max_{i=1}^{24}(G_0(i))} \tag{11.a}$$

$$G_{0,N}(i) = \frac{\mathrm{G}_0(\mathrm{i})}{Max_{i=1}^{24}(G_0(i))} \tag{11.b}$$

The Fig. 10 shows $I_{15,N}$, $G_{0,N}$ and the corresponding difference G_d evaluated for some days at different weather conditions during the period of low solar irradiance and highest weather variability. The solar irradiance difference G_d has a regular trend, which is quite similar to the extraterrestrial solar irradiance G_0 on the sunny days (November 14th 2012, December 23th 2012, January 19th 2013). Instead some sudden fluctuations of the solar irradiance difference G_d are evident on the cloudy days (November 20st, December 2nd 2012 and January 14th 2013). Furthermore the solar irradiance difference G_d can be identified as a parameter to extract information about several weather conditions starting from the measured solar irradiance.

For the previous analyzed days, the cross correlation coefficient R_{TP}(%) has been reported in the Table 10 for three sunny days (November 14th 2012, December 23th 2012, January 19th 2013) and three cloudy days (November 20st, December 2nd 2012, January 14th 2013). It’s noted that the cross correlation coefficient is higher on the sunny days than cloudy days. The forecasted PV power values, predicted by each method, are in good agreement with the measured values for the sunny day, instead the predicted power values have low correlation with the measured data under cloudy weather conditions. Furthermore, for long prediction time, the hybrid LS-SVM with WD method outperforms other models, in particular at cloudy days with R_{TP} values between 47,33% - 66,88% against 11,20% - 24,90% obtained with the ANN and 18,43% - 28,29% with the LS-SVM.. The Model III seems to be less influenced by cloudy weather conditions, giving the best performance.

5.3 Impact of forecasting accuracy on imbalance costs

A preliminary analysis has been carried out to evaluate the economic impact of the forecasting accuracy of the three methods, focusing the analysis on the PV dispatched energy in the electric grids. According to the Italian energies policy, the producers of renewable sources energy can participate in electric market through a programmed transactions. In the Day-Ahead Market the amount of energy that can be injected into the grid (Injection Schedule) is established for each hour of the next day, so the producers declare the quantity of energy to insert into the network with a day in advance. However, the unbalancing charges are applied when there is a difference between actual and scheduled injected energy [65]. The aim of the present analysis is to characterize three forecast models in terms of penalties for imbalance energy, adopting the approach used in [54] to calculate the penalties for imbalance. Hence, the actual energy (E_T) is remunerated at the producer with a energy price C_E, established on base of the Day-Ahead Market, if it is in the range [-10%;10%] of the energy declared (E_P) in the injection schedule (Case A). Otherwise, for each hour i a penalty C_I is applied to the amount energy equal to the gap between the actual E_T and the schedule E_P energy. Therefore, if E_T has been underestimated that means the schedule energy is higher than the energy actually injections into the electric grid (E_P), the producer must repay the missing energy at a price equal to C_E+C_I (Case B). If E_T has been overestimated that means the actual energy injected into the electric grid is higher than the schedule energy, the surplus energy is remunerated at the producer with a price equal to C_E-C_I (Case C).

Even if the energy price is influenced by the demand of energy [66], in this analysis, the energy price C_E is assumed constant for each day and hour and equal to 10c€/kWh and C_I is considerated equal to 50% of the energy price C_E. Hence, for each hour i and all possible cases, the economic flow is defined as follows:

A. $F(i) = C_E * E_T(i)$ when $|E_P - E_T| > 10\% E_P$

B. $F(i) = C_E * E_T(i) + (C_E + C_I) * (E_T(i) - E_P(i))$ when $E_P > E_T$

C. $F(i) = C_E * E_T(i) + (C_E - C_I) * (E_T(i) - E_P(i))$ when $E_P < E_T$

Fig. 11.a shows the percent occurrence of the different cases A, B, C (expressed on the total number M). It's evident that the probability, in percent terms, to inject the energy in the network within the admitted tolerance is quite low (10% - 15%). The probability to inject less energy than schedule (case A) is higher for the ANN and LS-SVM models, equal to 45% against 19,6% for the hybrid LS-SVM with WD. This entails greater costs at the producer because of the penalties for imbalance energy. The probability to inject more energy than schedule (case C) is higher for the model III (70,9%). It means that the LS-SVM with wavelet decomposition models allows to obtain the additional revenue, which corresponds to the energy that was not considered in the day-ahead schedule proposed by the producer.

Finally, the Fig. 11.b shows the total economic incomes, as the sum of the incomes of the case A, B and C for the three forecast models, normalized with the maximum economic revenue that is obtained from the remuneration of the injected actual energy at the price C_E (case A). It is evident that the LS-SVM with WD model guarantees the higher economic income, equal to 72,6%, than the ANN e LS-SVM models, approximately 53% for both. So, the results demonstrate that the LS-SVM with Wavelet Decomposition model has the lowest economics impact in terms of penality and the highest additional income, derived from its tendency to underestimate the PV power. Hence it allows to obtained the greatest revenue.

6. CONCLUSIONS

This study is focused on the implementations of innovative short-term forecasting systems based on Artificial Neural Networks (ANNs), Least Square Support Vector Machines (LS-SVMs) and hybridized LS-SVMs for photovoltaic power prediction of a site located in Apulia region – South East of Italy.

A detailed comparison between the ANN model and LS-SVM with and without the Wavelet Decomposition of the input dataset was carried out, analyzing the normalized mean error and the statistical distribution, to identify the most accurate forecasting method.

The evaluation of the performance of different forecasting methods is performed by the estimation of conventional metrics, as the root mean square error (RMSE), mean bias error (MBE), and mean absolute error (MAE).

High prediction errors were obtained from all forecasting methods at long time horizons. Observing the normalized error, the LS-SVM based models reach better performance than the ANN model but the hybrid LS-SVM based on the Wavelet Decomposition of the input data outperforms other models particularly for long forecasting horizons.

In the present work a deep error analysis was performed. A study of the statistical distributions of the normalized error was performed. In most cases, the probability that the normalized error take values in the ranges [-1%; +1%] is basically lower for the artificial neural networks and the probability to reach an error less than 20% is generally higher in the hybrid LS-SVM with Wavelet Transform. The decomposition of the root mean squared error into three contributions (bias, standard deviation bias and dispersion) and the estimation of the skewness, and kurtosis statistical metrics provide a better understanding of the differences between prediction and measurement. As might be expected, the short time ahead forecasts have much higher kurtosis values than those made at the day-ahead timescale. This would be expected from the reduction in uncertainty that occurs between making a forecast in the day-ahead time frame, versus a single hour ahead.

The bias can be subtracted and the standard deviation can be adjusted by increasing or decreasing the standard deviation of the prediction, contrary to the dispersion error. Therefore the reduction of the dispersion error constitutes the challenge for further improvements; hence forecasting methods with low dispersion error permit to reach a better accuracy. The analysis showed that the reduction in the dispersion is mainly due to the implementation of the Wavelet Decomposition rather than to the choice of the LS-SVM or ANN.

The impact of the solar irradiance fluctuation on the forecasting accuracy is also discussed. The use of Model III (LS-SVM with WD) leads to an improve of the accuracy, in particular in the cloudy days, which means that the decomposition of the input data permits better to take into account the solar irradiance fluctuations. Hence further work will implement the difference between the measured solar irradiance and the corresponding extraterrestrial solar irradiance, as an input of the forecasting method.

Finally an analysis was performed to evaluate the penalties for unbalancing energy of three forecast models, concluding that the LS-SVM with Wavelet Decomposition Technique model also permits to reach the greatest revenue with lower costs for unbalancing penality with respect to the ANN and the LS-SVM.

Funds

This work is supported by the Project BEAMS, Project Number 285194, 7th Framework Program.

Acknowledgments

The authors would like to thank Elettrostudio Energia SpA and Esapro Advanced Energy Service for their kind availability and for the possibility to access data.

Conflict of interest statement

The paper and its corresponding work is completed by all the authors. No conflict of copyright is involved.

REFERENCES

[1] Congedo PM, Malvoni M, Mele M, De Giorgi MG. Performance measurements of monocrystalline silicon PV modules in South-eastern Italy. Energy Conversion and Management 2013; 68:1-10.

[2] De Giorgi MG, Congedo PM, Malvoni M, Tarantino M. Short-term power forecasting by statistical methods for photovoltaic plants in south Italy. In: 4th IMEKO TC19 Symposium on Environmental Instrumentation and Measurements: Protection Environment, Climate Changes and Pollution Control, June 3-4, Lecce, Italy, 2013. p 171-175.

[3] Mellit A, Eleuch H, Benghanem M, Elaoun C, Pavan A. An adaptive model for predicting of global, direct and diffuse hourly solar irradiance. Energy Conversion and Management 2010; 51:771-782.

[4] Mellit A, Pavan AM. A 24-h forecast of solar irradiance using artificial neural network: Application for performance prediction of a grid-connected PV plant at Trieste, Italy. Solar Energy 2010; 84:807-821.

[5] Su Y, Chan LC, Li Y, Tsui KL. Real-time prediction models for output power and efficiency of grid-connected solar photovoltaic systems. Applied Energy 2012; 93:319-326.

[6] Lei M, Shiyan L, Chuanwen J, Hongling L, Yang Z. A review on the forecasting of wind speed and generated power. Renewable & Sustainable Energy Reviews 2009; 13(4): 915-920.

[7] More A, Deo MC. Forecasting wind with neural networks. Marine Structures 2003; 16(1): 35-49.

[8] Gareta R, Romeo LM, Gil A. Forecasting of electricity prices with neural networks. Energy Conversion and Management 2006; 47 (13-14): 1770-1778.

[9] Ardakani FJ, Ardehali MM. Novel effects of demand side management data on accuracy of electrical energy consumption modeling and long-term forecasting. Energy Conversion and Management 2014; 78: 745-752.

[10] Nagi J, Yap KS, Tiong SK, Ahmend SK. Electrical Power Load Forecasting using Hybrid Self-Organizing Maps and Support Data Machine. In: Proc. of the 2nd International Power Engineering and Optimization Conference (PEOCO), June 4-5, Shah Alam, Malaysia, 2008, pp. 51–56.

[11] De Giorgi MG, Ficarella A, Russo MG. Short-term wind forecasting using artificial neural networks (ANNs). In: Second International Conference on Energy and Sustainability, June 23-25, Bologna, Italy, 2009.

[12] Velo R, López P, Maseda F. Wind speed estimation using multilayer perceptron. Energy Conversion and Management 2014; 81: 1-9.

[13] Almonacid F, Rus C, Hontoria L, Fuentes M, Nofuentes G. Characterisation of Si-crystalline PV modules by artificial neural networks. Renewable Energy 2009; 34: 941-949.

[14] Almonacid F, Rus C, Pérez-Higueras P, Hontoria L. Estimation of the energy of a PV generator using artificial neural network. Renewable Energy 2009; 34: 2743-2750.

[15] Almonacid F, Rus C, Pérez-Higueras P, Hontoria L. Calculation of the energy provided by a PV generator. Comparative study: Conventional methods vs. Artificial neural networks. Energy 2011; 36: 375-384.

[16] Alexiadis M. Short-term forecasting of wind speed and related electrical power. Solar Energy 1998; 63 (1): 61-68;

[17] Li G, Shi J. On comparing three artificial neural networks for wind speed forecasting Applied Energy 2010; 87 (7): 2313-2320.

[18] Cao Q, Ewing B, Thompson M. Forecasting wind speed with recurrent neural networks European Journal of Operational Research 2012; 221 (1): 148-154.

[19] Sfetsos A. A comparison of various forecasting techniques applied to mean hourly wind speed time series. Renewable Energy 2000; 21 (1): 23-35.

[20] Costa A, Crespo A, Navarro J, Lizcano G, Madsen H, Feitosa E. A review on the young history of the wind power short-term prediction. Renewable Sustain Energy Reviews 2008; 12 (6): 1725-1744.

[21] Pourmousavi Kani SA, Ardehali SA. Very short-term wind speed prediction: A new artificial neural network-Markov chain model. Energy Conversion and Management 2011: 52: 738-745.

[22] Bonanno F, Capizzi G, Graditi G, Napoli C, Tina GM. A radial basis function neural network based approach for the electrical characteristics estimation of a photovoltaic module. Applied Energy 2012; 97: 956-961.

[23] Rus-Casas C, Aguilar J, Rodrigo P, Almonacid F, Pérez-Higueras P. Classification of methods for annual energy harvesting calculations of photovoltaic generators. Energy Conversion and Management 2014; 78: 527-536.

[24] Fadare DA. The application of artificial neural networks to mapping of wind speed profile for energy application in Nigeria. Applied Energy 2010; 87 (3): 934–942.

[25] Fadare DA. Modelling of solar energy potential in Nigeria using an artificial neural network model. Applied Energy 2009; 86: 1410-1422.

[26] Kariniotakis GN, Stavrakakis GS, Nogaret EF. Wind power forecasting using advanced neural networks models. IEEE Trans Energy Conversion 1996; 11 (4): 762-767.

[27] De Giorgi MG, Ficarella A, Tarantino M. Error analysis of short term wind power prediction models. Applied Energy 2011; 88:1298-1311.

[28] Yona A, Senjyu T, Funabashi T. Application of Recurrent Neural Network to Short-Term-Ahead Generating Power Forecasting for Photovoltaic System. In: Power Engineering Society General Meeting, 24-28 June, Tampa, FL, 2007. pp. 1-6.

[29] Dorvlo ASS, Jervase JA, Lawati AA. Solar radiation estimation using artificial neural networks, Applied Energy 2002; 71:307-319.

[30] Benmouiza K, Cheknane A, Forecasting hourly global solar radiation using hybrid k-means and nonlinear autoregressive neural network models, Energy Conversion and Management 2013; 75: 561-569.

[31] Ali N. Celik, Muneer T, Neural network based method for conversion of solar radiation data, Energy Conversion and Management 2013; 67: 117-124.

[32] Chupong C, Plangklang B. Forecasting power output of PV grid connected system in Thailand without using solar radiation measurement. Energy Procedia 2011; 9:230-237.

[33] Vapnik VN. The Nature of Statistical Learning Theory. Springer-Verlag, New York, 1995, ISBN 978-0-387-98780-4.

[34] Vapnik VN, Statistical Learning Theory (Adaptive and Learning Systems for Signal Processing, Communications and Control Series), Wiley, New York, 1998.

[35] Junping W, Quanshi C, Binggang C, Support vector machine based battery model for electric vehicles, Energy Conversion and Management 2006, 47:858-864.

[36] Pai PF, Hong WC. Support vector machines with simulated annealing algorithms in electricity load forecasting. Energy Conversion and Management 2005; 46:2669-2688.

[37] Sreelakshmi K, Kumar PR. Performance evaluation of short term wind speed prediction techniques, IJCSNS International Journal of Computer Science and Network Security, August 2008, Vol 8, pp 162-9.

[38] Mohandes M, Halawani T, Rehman S, Hussain A. Support vector machines for wind speed prediction. Renewable Energy 2004; 29:939-47.

[39] Chen JL, Li SL, Wu SJ. Assessing the potential of support vector machine for estimating daily solar radiation using sunshine duration. Energy Conversion and Management 2013; 75:311-318.

[40] Chen J, H, Wu W, Xie D. Estimation of monthly solar radiation from measured temperature using support vector machines e a case study. Renewable Energy 2011; 36:413-20.

[41] S. Fonseca JG, Oozeki T, Takashima T, Koshimizu G, Uchida Y, Ogimoto K. Photovoltaic power production forecasts with support vector regression: A study on the forecast horizon. In: 37th IEEE Photovoltaic Specialists Conference, 19-24 June 2011, pp.2579-2583.

[42] Fan S, Chen L, Lee WL, Machine learning based switching model for electricity load forecasting, Energy Conversion and Management 2008, 49: 1331-1344.

[43] Fan S; Chen L. Short-term load forecasting based on an adaptive hybrid method. In: IEEE Trans. Power Syst., vol. 21, no. 1, pp. 392–401, Feb. 2006.

[44] Suykens JAK, Van Gestel T, Debrebanter J. Least Squares Support Vector Machines. Singapore: World Scientific Publishing Co., 2002.

[45] Huang CY, Chiang BY, Chang SY, Tzeng GH, Tseng CC. Predicting of the Short Term Wind Speed by Using a Real Valued Genetic Algorithm Based Least Squared Support Data Machine. Intelligent Decision Technologies Smart Innovation, Systems and Technologies, Vol. 10, 2011, pp 567-575.

[46] Zhou J, Shi J, Li G. Fine tuning support vector machines for short-term wind speed forecasting. Energy Conversion and Management 2011; 52:1990-1998.

[47] De Giorgi MG, Campilongo S, Ficarella A, Congedo PM. Comparison Between Wind Power Prediction Models Based on Wavelet Decomposition with Least-Squares Support Vector Machine (LS-SVM) and Artificial Neural Network (ANN). Energies 2014; 7(8): 5251-5272.

[48] Mallat SG. A theory for multiresolution signal decomposition: the wavelet representation. In: IEEE Transactions on pattern analysis and machine intelligence, Jul 1989, vol.11, no.7, pp.674-693.

[49] De Giorgi MG, Ficarella A, Tarantino M. Assessment of the benefits of numerical weather predictions in wind power forecasting based on statistical methods. Energy 2011; 36:3968-3978.

[50] Shayeghi H, Ghasem, A. Day-ahead electricity prices forecasting by a modified CGSA technique and hybrid WT in LSSVM based scheme. Energy Conversion and Management 2013; 74: 482-491.

[51] Amjady N, Keynia F. Short-term load forecasting of power systems by combination of wavelet transform and neuro-evolutionary algorithm. Energy 2009; 34:46-57.

[52] Motevasel M, Seifi AR. Expert energy management of a micro-grid considering wind energy uncertainty Energy Conversion and Management 2014; 83: 58-72.

[53] Italian Authority for the Electricity Gas and Water, Resolution 522/14/R/eel. Disposizioni in materia di dispacciamento delle fonti rinnovabili non programmabili a seguito della sentenza del Consiglio di Stato. 2014. Sezione Sesta-9 giugno 2014, n. 2936

[54] Delfanti M, Falabretti D, Merlo M. Energy storage for PV power plant dispatching. Renewable Energy 2015; 80: 61-72.

[55] De Giorgi MG, Congedo PM, Malvoni M. Photovoltaic power forecasting using statistical methods: impact of weather data. IET Science, Measurement and Technology, pp 1–8, doi: 10.1049/iet-smt.2013.0135.

[56] http://supervisione.espe.it/fotovoltaicoWeb/index.htm.

[57] Madsen H, Pinson P, Kariniotakis G, Nielsen HA, Nielsen TS. Standardizing the performance evaluation of short-term wind power prediction models. Wind Energy 2005; 29:475-89.

[58] Carlos FM, Kleissl C, Kleissl J, Marquez R. Solar Energy Forecasting and Resource Assessment. Elsevier 2013 ISBN: 9780123971777.

[59] Lange M. On the Uncertainty of Wind Power Predictions - Analysis of the Forecast Accuracy and Statistical Distribution of Errors. Journal of Solar Energy Engineering 2005; 127(2): 177-184.

[60] Chiang YM, Chang LC, Chang FJ. Comparison of static-feedforward and dynamic-feedback neural networks for rainfall–runoff modeling. Journal of Hydrology 2004; 290: 297–311.

[61] Hecht-Nielsen R. Theory of the back-propagation neural network, IEEE IJCNN, 1989 Vol.1 pp 593 – 605.

[62] Duffie JA, Beckman WA. Solar Engineering of Thermal Processes: Fourth Edition (2013) DOI: 10.1002/9781118671603.

[63] Table 1.6.1 of [62].

[64] http://www.solaritaly.enea.it/StrDiagrammiSolari/X12Mesi1.php

[65] https://www.mercatoelettrico.org/en/tools/Glossario.aspx

[66] He YX, Liu YY, Xia T, Zhou B. Estimation of demand response to energy price signals in energy consumption behaviour in Beijing, China. Energy Conversion and Management 2014; 80. 429 -435.

LIST OF TABLE

Table 1 Technical specifications of the PV module and system

Module	
Type	Mono-crystalline silicon
Nominal power (P_n)	960 kW_p
Maximum power voltage (V_{pm})	3000 V
Maximum power current (I_{pm})	3 A
Open circuit voltage (V_{oc})	250 V
Short circuit current (I_{sc})	12 A
Weight	4710 m^2 [4892 m^2]
Net [gross] module surface	1.57 m^2 [1.63 m^2]
Subfield	
PV1	
Nominal power of PV system	353.3 kW_p
Azimuth	-10°
Tilt	3°
Total number of modules	1104
Net [gross] modules' surface	1733.3 m^2 [1799.5 m^2]
PV2	
Nominal power of PV system	606.7 kW_p
Azimuth	-10°
Tilt	15°
Total number of modules	1896
Net [gross] modules' surface	2976.7 m^2 [3090.5 m^2]

Table 2 Measured data used as forecast factors

Symbol	*Unit*	*Description*
P	kW	Instantaneous AC power
T_m	°C	Module Temperature
T_a	°C	Ambient Temperature
I_3	W/m^2	Irradiance on plane of module with tilt 3°
I_{15}	W/m^2	Irradiance on plain of module with tilt 15°

Table 3 Elman ANN settings

		Input Vector 1	*Input Vector 2*
Training function		TRAINGDX Gradient descent with momentum and adaptive learning rate back-propagation	
Adapt learning function		LEARNGD Gradient descent weight and bias learning function	
Performance function		MSE Mean Squared Error	
Number layers		3	
Neurons (layer 1)	*1h*	21	16
	3h	31	26
	6h	61	51
	12h	121	101
	24h	241	201
Neurons (layer 2)	*1h*	11	8
	3h	16	13
	6h	31	26
	12h	61	51
	24h	121	101
Neurons (layer 3) – output		1	
Activation function hidden layer		TANSIG Hyperbolic tangent sigmoid transfer function	
Activation function output layer		PURELIN Linear transfer function	
Epochs		500	

Table 4 Acronym used to indicate the combination forecast methods and input vectors

Model	*Description*
I.1	Elman Back - Propagation ANN with input vector 1 (IV1)
I.2	Elman Back - Propagation ANN with input vector 2 (IV2)
II.1	Least Square – Support Data Machine (LS-SVM) with input vector 1 (IV1)
II.2	Least Square – Support Data Machine (LS-SVM) with input vector 2 (IV2)
III.1	LS-SVM with Daubechies type 4 Wavelet Decomposition on 8 levels with input vector 1 (IV1)
III.2	LS-SVM with Daubechies type 4 Wavelet Decomposition on 8 levels with input vector 2 (IV2)

Table 5 NMBE, NMAE and NRMSE values given by Model I, II and III

	Model I		*Model II*		*Model III*	
Horizon	***Input vector 1***	***Input vector 2***	***Input vector 1***	***Input vector 2***	***Input vector 1***	***Input vector 2***
			NMBE(%)			
1	-3,50%	0,72%	-1,33%	1,06%	0,12%	-2,50%
3	-5,23%	1,44%	-2,26%	1,48%	1,50%	-3,79%
6	-8,44%	-0,21%	-4,59%	5,27%	3,85%	0,45%
12	-9,27%	-1,25%	-9,25%	-1,20%	6,04%	-1,41%
24	-3,42%	-2,55%	-3,43%	-3,15%	1,16%	13,40%
			NMAE(%)			
1	9,40%	6,50%	7,53%	6,40%	6,57%	6,92%
3	15,11%	10,86%	13,62%	10,18%	10,77%	10,35%
6	20,18%	13,79%	18,22%	13,50%	13,53%	10,53%
12	21,12%	14,38%	21,11%	14,53%	15,04%	14,22%
24	25,05%	19,49%	23,52%	19,50%	18,91%	19,00%
			NRMSE(%)			
1	12,57%	10,91%	12,14%	11,12%	10,66%	9,60%
3	18,55%	15,61%	17,97%	15,79%	15,93%	14,09%
6	23,11%	18,89%	22,07%	21,24%	19,65%	15,28%
12	23,69%	18,80%	22,89%	19,73%	16,32%	18,76%
24	26,20%	23,99%	23,68%	24,07%	20,86%	22,76%

Table 6 Value of the amplitude and phase error

	Model I		***Model II***		***Model III***	
Horizon	***Input vector 1***	***Input vector 2***	***Input vector 1***	***Input vector 2***	***Input vector 1***	***Input vector 2***
			SDE			
1	0,12	0,11	0,12	0,11	0,11	0,09
3	0,18	0,16	0,18	0,16	0,16	0,14
6	0,22	0,19	0,21	0,21	0,19	0,15
12	0,22	0,19	0,21	0,20	0,20	0,19
24	0,23	0,24	0,23	0,24	0,21	0,20
			SD_{bias}			
1	-0,023	-0,016	-0,018	-0,019	-0,026	-0,028
3	-0,060	-0,036	-0,058	-0,040	-0,065	-0,029
6	-0,107	-0,062	-0,106	-0,082	-0,114	-0,042
12	-0,182	-0,098	-0,182	-0,091	-0,136	-0,100
24	-0,201	-0,153	-0,201	-0,148	-0,146	-0,135
			DISP			
1	0,119	0,108	0,119	0,109	0,104	0,089
3	0,168	0,151	0,169	0,152	0,145	0,133
6	0,186	0,179	0,188	0,189	0,156	0,147
12	0,121	0,160	0,120	0,174	0,146	0,158
24	0,105	0,183	0,104	0,187	0,154	0,148

Table 7 Measures of Skewness and Kurtosis

	Model I		*Model II*		*Model III*	
Horizon	***Input vector 1***	***Input vector 2***	***Input vector 1***	***Input vector 2***	***Input vector 1***	***Input vector 2***
			SKEW			
1	0,674	0,710	0,301	0,528	0,274	0,634
3	1,029	0,769	1,012	0,580	0,564	0,266
6	1,423	1,130	1,430	1,283	0,919	0,669
12	1,457	1,373	1,457	1,182	0,911	1,406
24	-0,126	-0,071	-0,129	-0,078	-0,258	-0,319
			KURT			
1	2,827	4,581	2,616	5,053	2,509	2,299
3	1,433	1,648	1,442	2,744	0,868	1,070
6	1,595	1,625	1,619	2,395	0,584	2,166
12	1,387	1,967	1,388	2,129	0,639	2,060
24	-0,610	-0,396	-0,608	-0,371	0,315	-0,460

Table 8 Error distribution of forecast models at different prediction length (1h, 6h and 12h)

	Model I		*Model II*		*Model III*	
Horizon	***Input vector 1***	***Input vector 2***	***Input vector 1***	***Input vector 2***	***Input vector 1***	***Input vector 2***
			[-1% - +1%]			
1	2,48%	28,94%	**44,65%**	37,85%	35,53%	20,88%
6	1,32%	10,91%	1,11%	17,19%	**22,25%**	18,56%
12	2,11%	6,96%	1,95%	10,17%	10,60%	**17,82%**
			[-5% - +5%]			
1	16,39%	**63,52%**	56,83%	61,78%	60,04%	48,29%
6	5,90%	26,83%	5,27%	**41,12%**	36,69%	39,38%
12	8,12%	21,24%	8,12%	24,62%	28,26%	**35,00%**
			[-10% - +10%]			
1	71,64%	**77,65%**	69,53%	76,91%	74,17%	73,59%
6	11,65%	53,08%	11,81%	58,04%	51,98%	**59,99%**
12	16,76%	43,91%	16,71%	43,96%	46,39%	**54,14%**
			[-20% - +20%]			
1	87,08%	90,83%	87,66%	91,09%	90,77%	**94,89%**
6	66,63%	77,86%	70,16%	77,12%	74,17%	**83,71%**
12	36,85%	77,91%	36,85%	74,80%	73,43%	**78,55%**

Table 9 The extraterrestrial solar irradiance for the investigated site (Lat. 40°21' Log. 18°11')

Month / *Hour*	*17 Jan*	*16 Feb*	*16 Mar*	*15 Apr*	*15 May*	*11 Jun*	*17 July*	*16 Aug*	*15 Sep*	*15 Oct*	*14 Nov*	*10 Dec*
03:00 AM												
04:00 AM												
05:00 CET					99,98	153,98	100,47					
06:00 AM				203,60	366,20	414,75	353,80	252,49	129,95			
07:00 AM		58,89	254,67	472,30	624,12	667,29	619,91	518,23	401,06	256,85	99,49	
08:00 AM	180,63	311,08	493,66	690,26	805,55	840,06	808,31	740,70	635,92	501,30	326,28	206,47
09:00 AM	392,78	534,47	734,25	935,14	1058,26	1097,88	1056,96	983,24	860,81	706,06	516,39	398,22
10:00 AM	551,76	706,27	899,35	1097,42	1205,18	1239,93	1213,20	1142,86	1019,38	840,95	651,82	537,89
11:00 AM	645,47	811,77	1005,46	1187,24	1292,32	1327,21	1304,80	1237,09	1104,36	917,09	728,98	620,58
12:00 AM	672,50	850,22	1038,78	1210,02	1308,08	1343,19	1330,29	1261,46	1119,71	926,80	730,46	627,43
01:00 PM	641,08	813,96	1000,09	1156,21	1248,21	1289,82	1287,75	1213,33	1065,18	854,50	664,42	576,16
02:00 PM	533,64	709,96	888,12	1032,31	1125,66	1176,17	1177,70	1097,39	931,49	714,37	531,51	449,09
03:00 PM	370,26	539,14	709,22	848,85	943,61	997,09	1008,01	922,34	746,59	517,21	343,99	277,31
04:00 PM	156,77	324,70	484,58	618,66	722,26	783,83	788,66	700,14	508,72	279,57	108,93	58,50
05:00 PM		76,67	224,64	362,37	474,89	543,75	548,24	440,84	246,41	12,96		
06:00 PM				83,94	205,85	290,76	293,38	176,59				
07:00 PM						36,51	36,28					
08:00 PM												
09:00 PM												

Table 10 The cross correlation coefficient R_{TP}(%)of prediction models at 3h and 12h forecast time horizons

		Model I		***Model II***		***Model III***	
		R_{TP} (%) +3h	***R_{TP}(%) +12h***	***R_{TP}(%) +3h***	***R_{TP}(%) +12h***	***R_{TP}(%) +3h***	***R_{TP}(%) +12h***
20 Nov	***Cloudy day***	57,18%	24,90%	62,18%	28,29%	74,89%	62,33%
14 Nov	***Sunny day***	83,81%	72,64%	86,91%	79,13%	92,86%	92,02%
2 Dic	***Cloudy day***	62,19%	17,62%	62,94%	22,72%	67,23%	66,88%
23 Dic	***Sunny day***	96,59%	86,00%	98,30%	87,23%	95,23%	92,84%
14 Jan	***Cloudy day***	63,65%	11,20%	72,10%	18,43%	85,80%	47,33%
19 Jan	***Sunny day***	98,36%	89,65%	97,55%	89,29%	95,70%	89,29%

Figure(s)

List of figures captions

Fig. 1. PV parking of the University of Salento.

Fig. 2. Conceptual chart of the implemented prediction models

Fig. 3. Measured vs forecasting PV power of a week of the February at the time horizon 1h using all models

Fig. 4. Comparison the normalized measured PV power with normalized error Ei at time horizon +6h using all models

Fig. 5. Comparison the normalized measured PV power with normalized error Ei at time horizon +12h using all models

Fig. 6. Trend of SDE2, DISP2 and SDbias2, implementing Equation (6.b) with IV2

Fig. 7. Probability distributions of normalized error for the model I, II and III with IV1 at a different time horizon

Fig. 8. Probability distributions of normalized error for the model I, II and III with IV2 at a different time horizon

Fig. 9. Probability that the normalized error takes values in the range a) [-1%; +1%] b) [-5%; +5%] c) [-10%; +10%] d) [-20%; +20%] using IV2

Fig. 10. Extraterrestrial solar irradiance, irradiance on module's plane and solar irradiance difference on days at different weather conditions

Fig. 11. Impact of penalties for imbalance energy

Figure 01
Click here to download high resolution image

Figure 02
Click here to download high resolution image

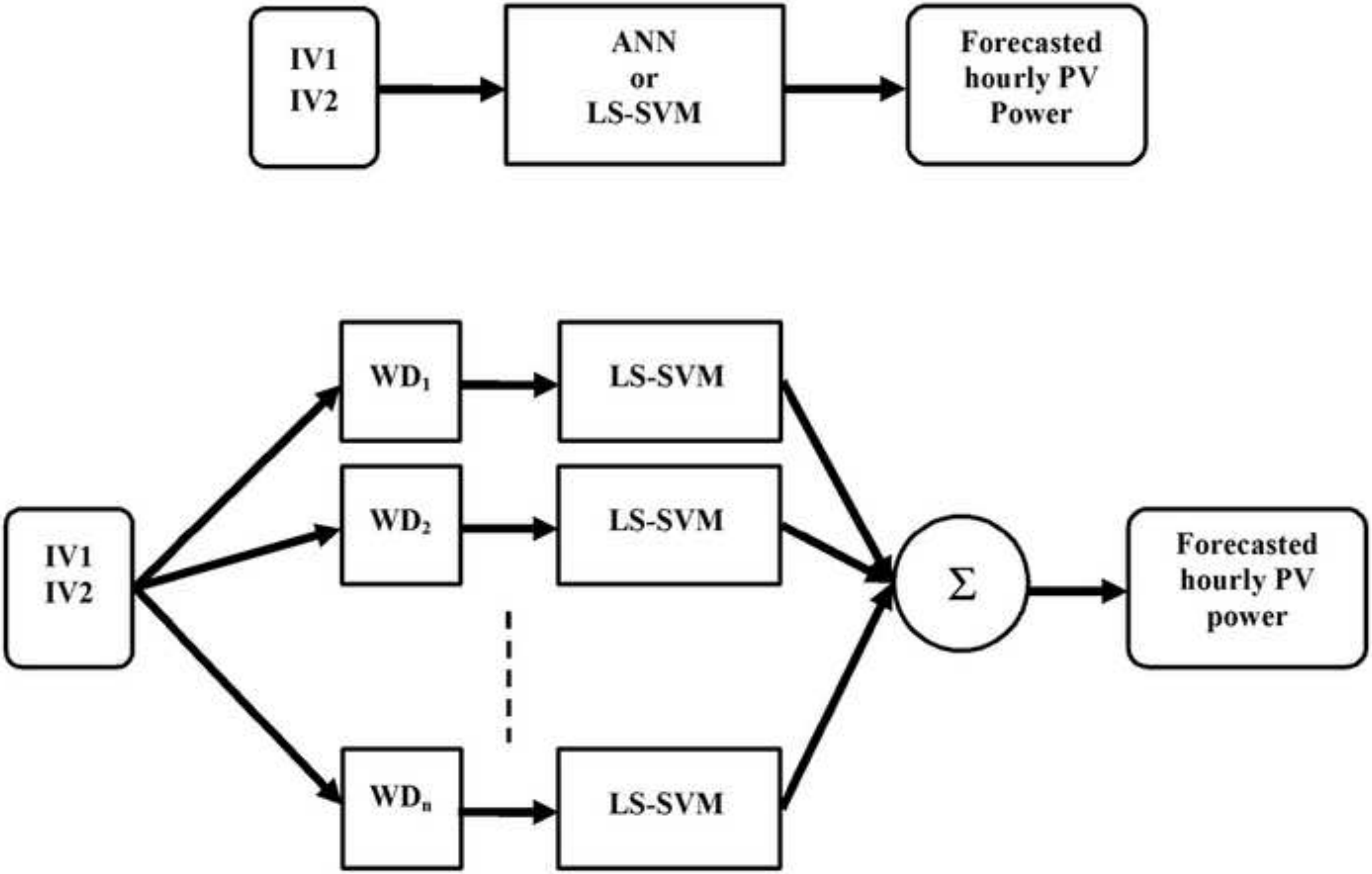

Figure 03
Click here to download high resolution image

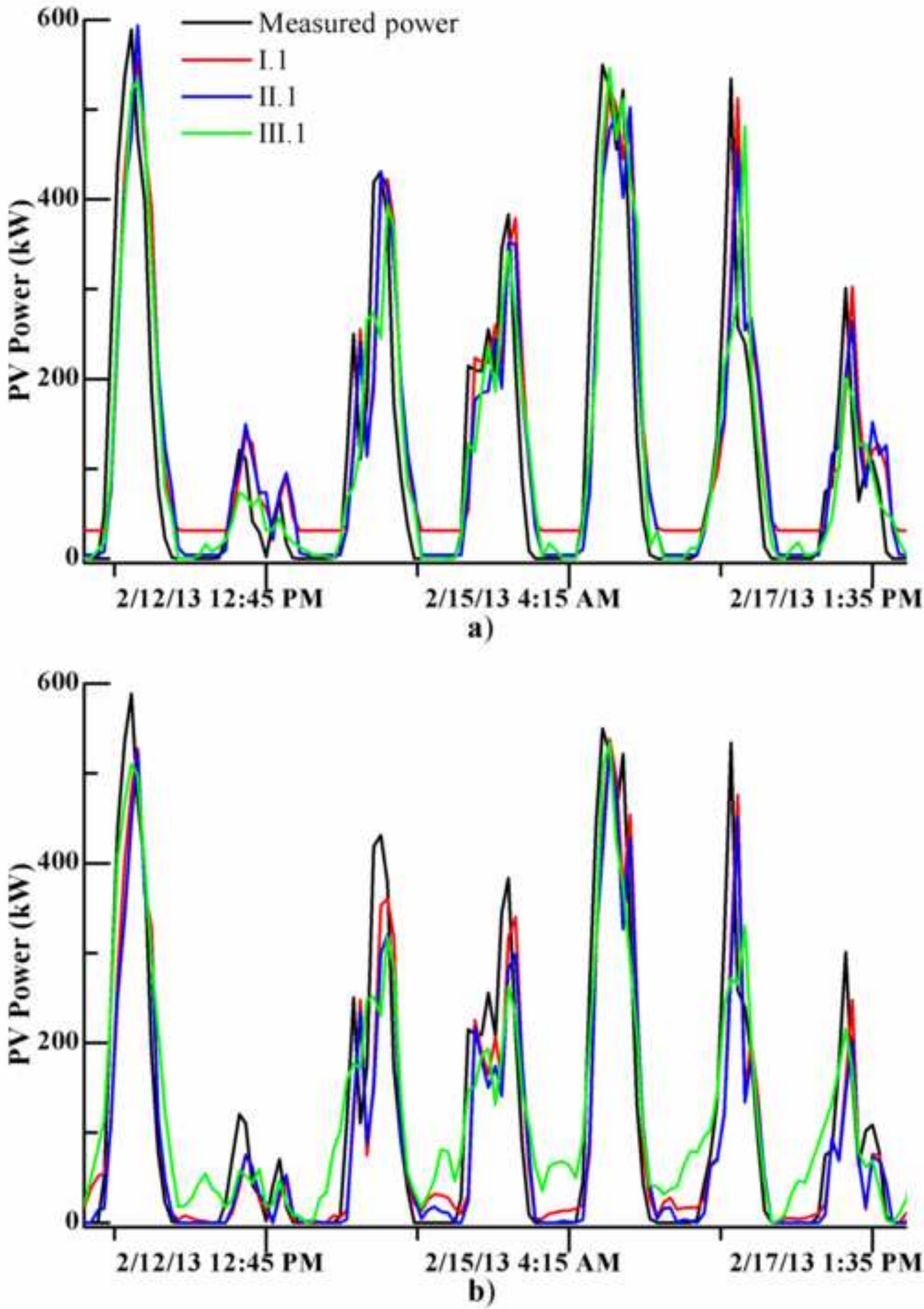

Figure 04
Click here to download high resolution image

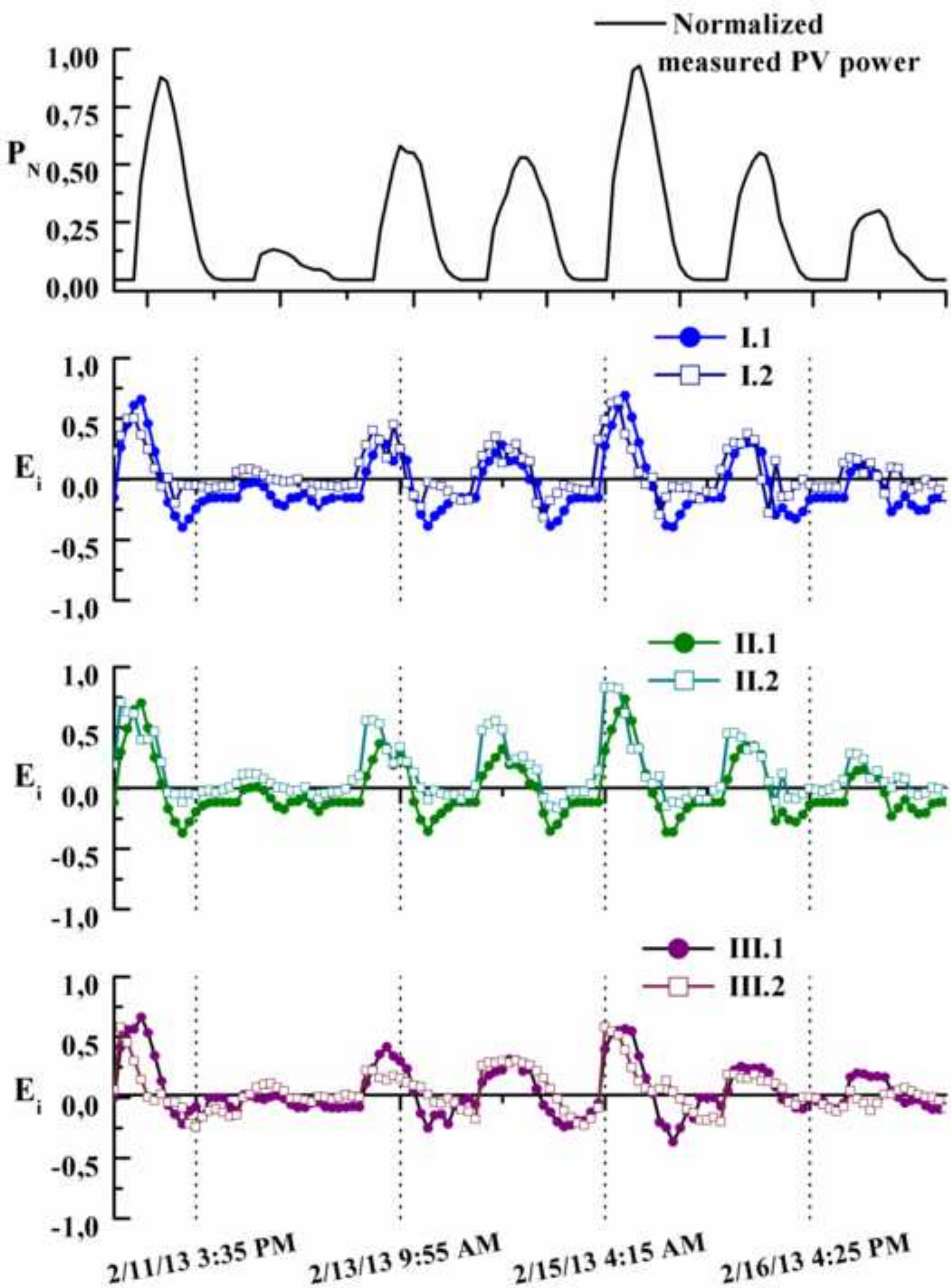

Figure 05
Click here to download high resolution image

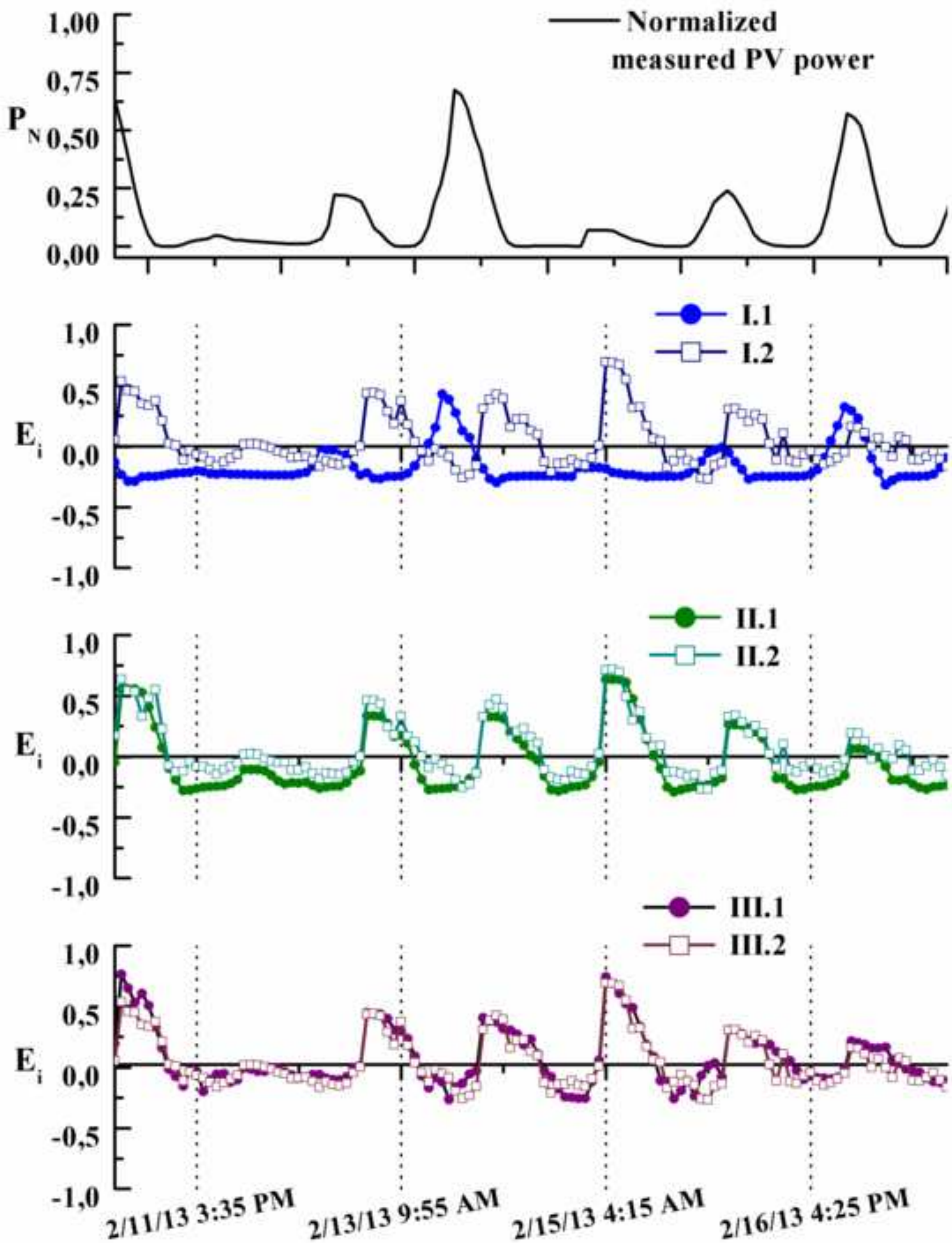

Figure 06
Click here to download high resolution image

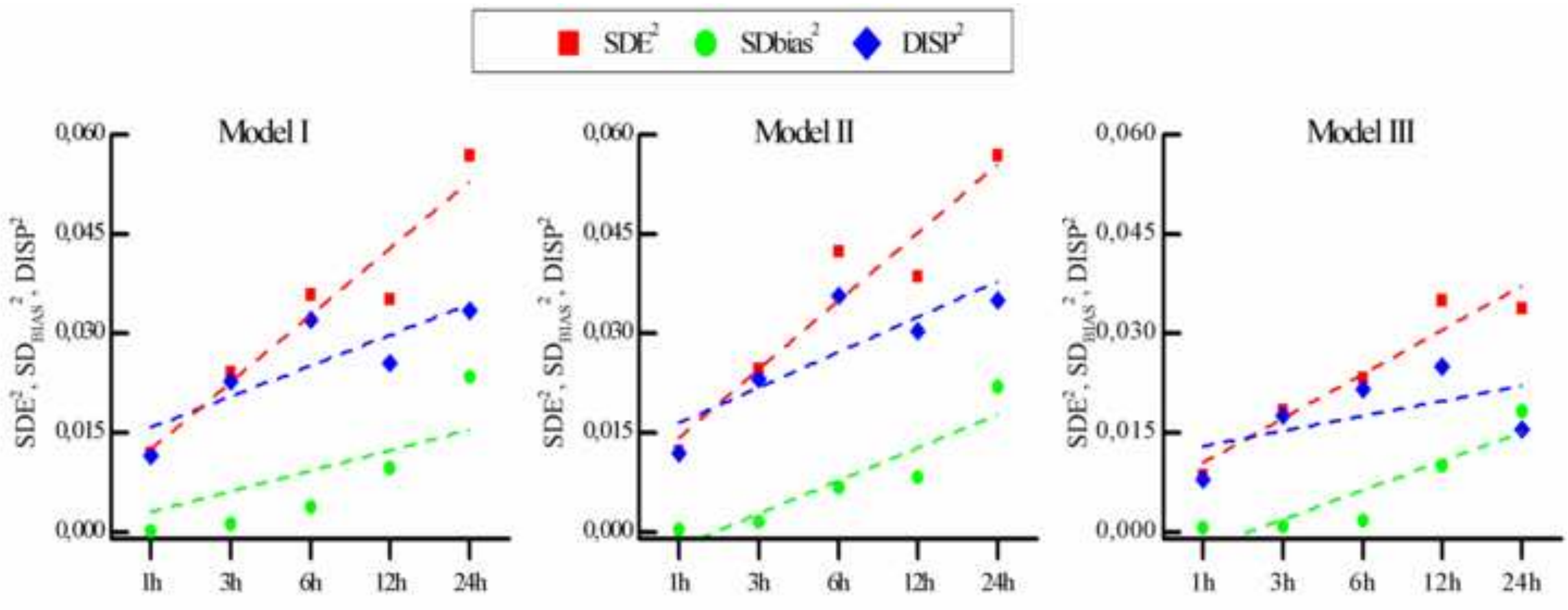

Figure 07
Click here to download high resolution image

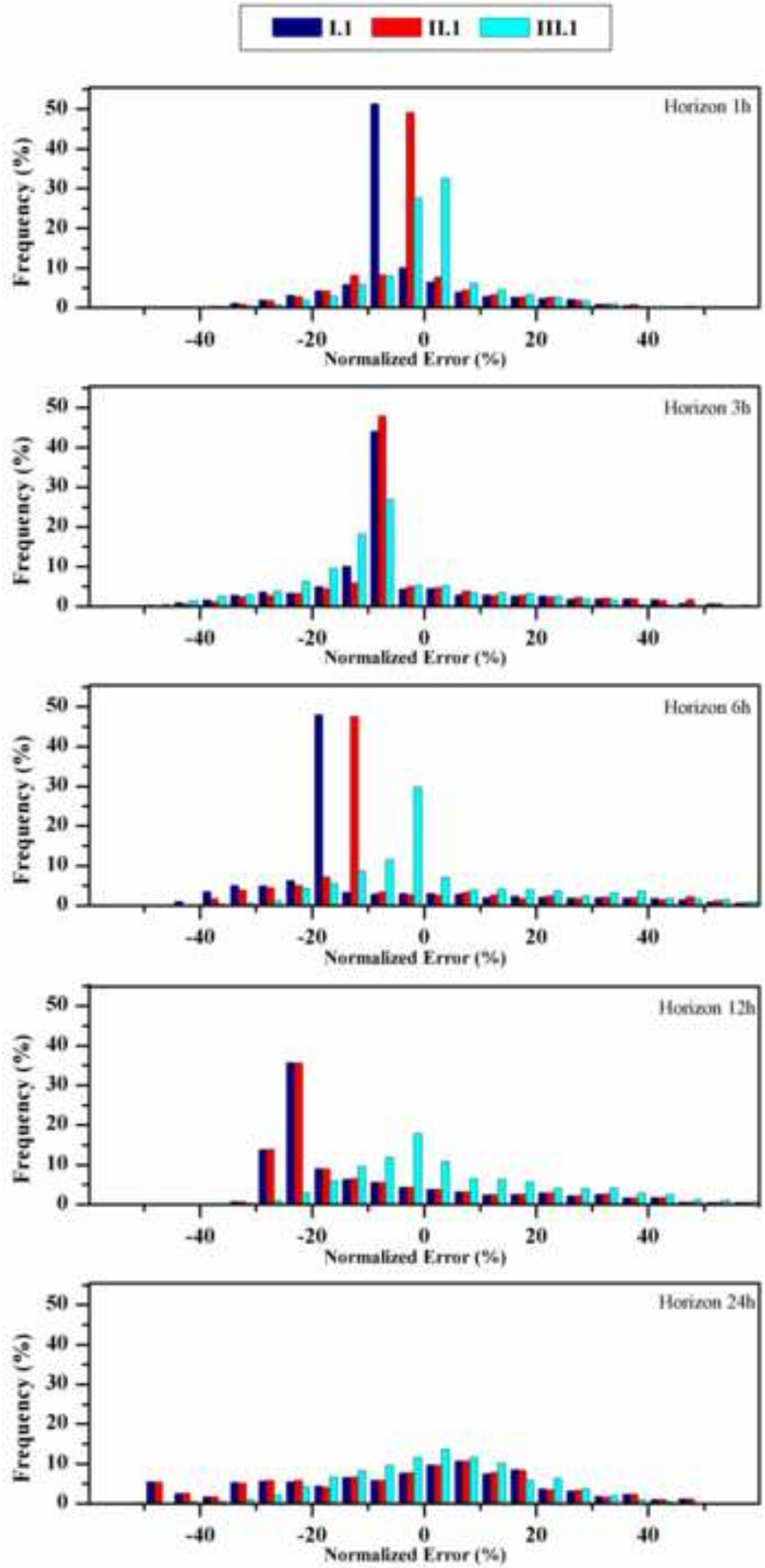

Figure 08
Click here to download high resolution image

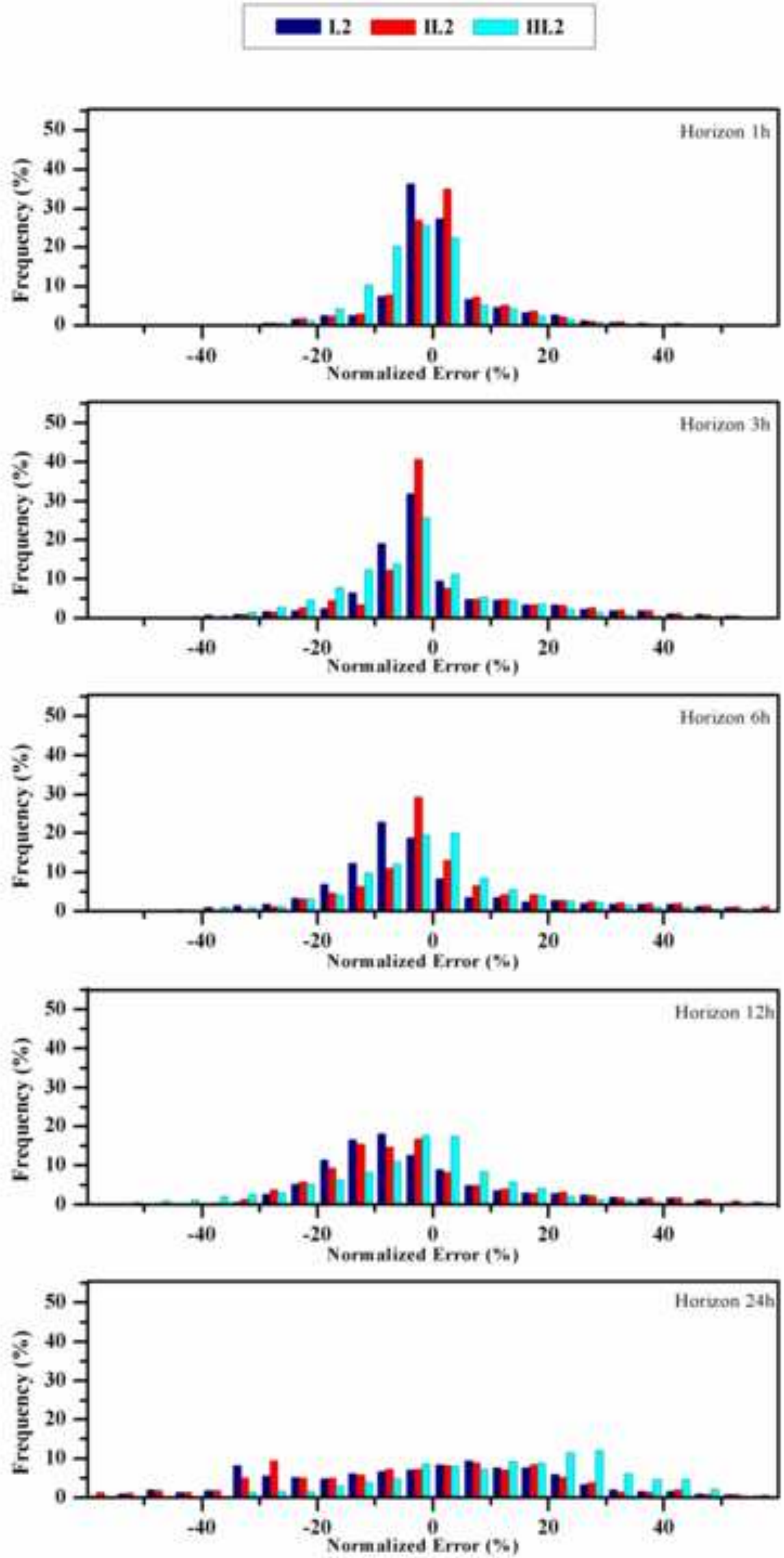

Figure 09
Click here to download high resolution image

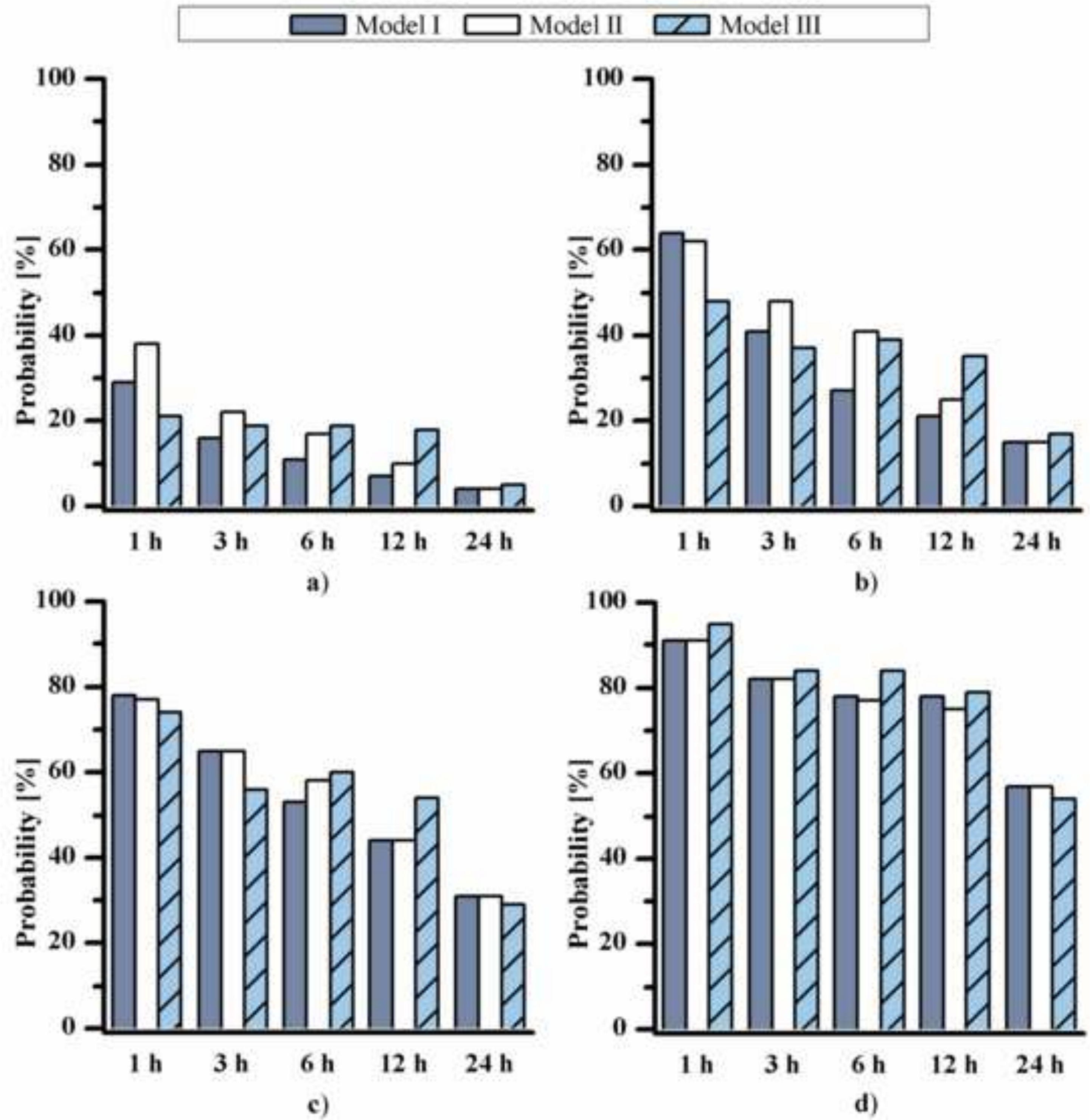

Figure 10
Click here to download high resolution image

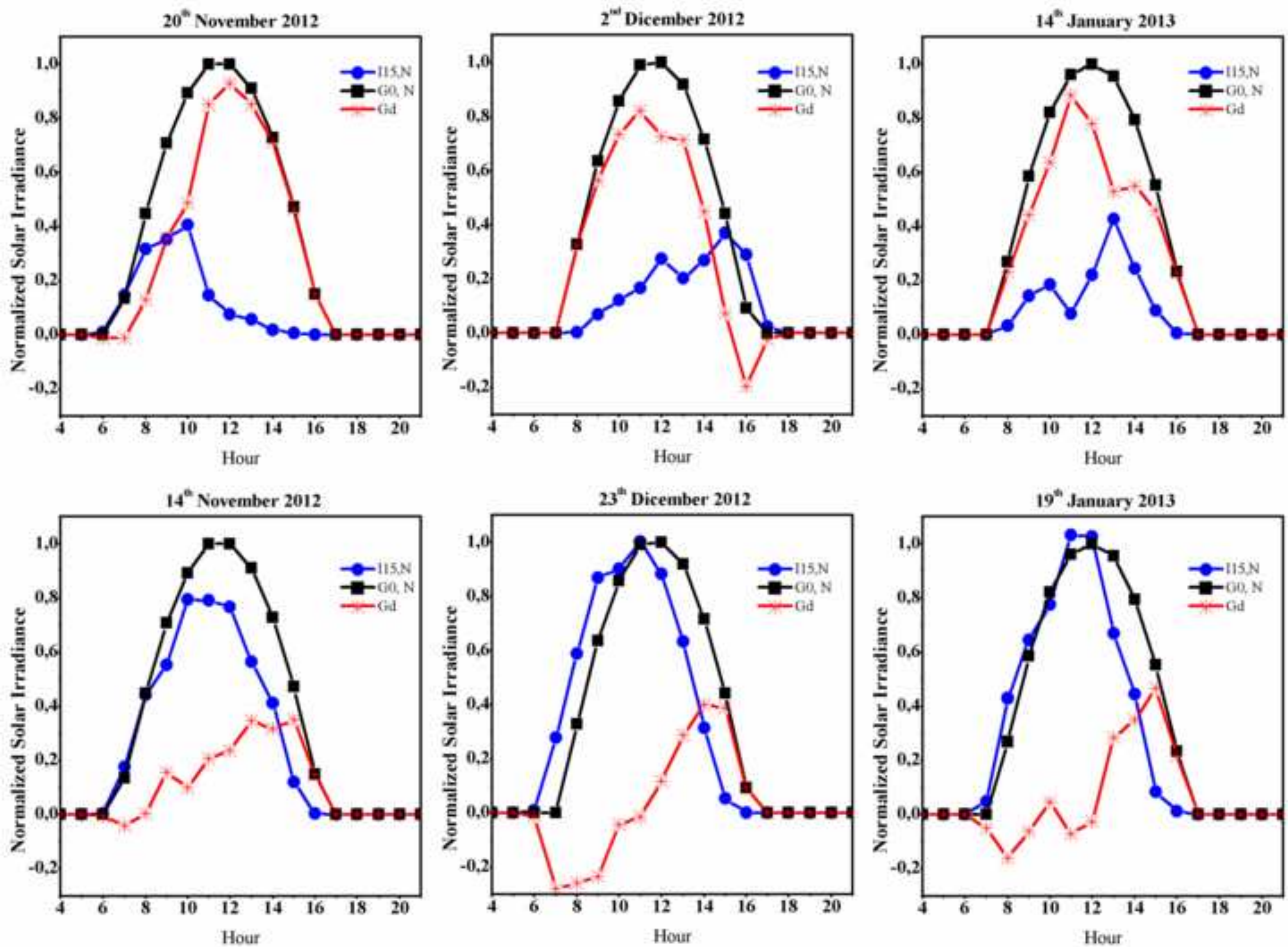

Figure 11
Click here to download high resolution image